JOURNAL OF MAGNETIC RESONANCE, Series A **116,** 196–205 (1995)

Two-Dimensional Fourier-Transform EPR Nutation Spectroscopy of Spin-Correlated Radical Pairs

RYUJI HANAISHI, YASUNORI OHBA, KIMIO AKIYAMA, SEIGO YAMAUCHI, AND MASAMOTO IWAIZUMI*

Institute for Chemical Reaction Science, Tohoku University, Katahira 2-1-1, Aoba, Sendai 980, Japan

Received January 3, 1995; revised May 12, 1995

The anomalous flip-angle dependence of the Fourier-transform EPR spectrum of photochemically generated spin-correlated radical pair (SCRP) was verified by means of a two-dimensional FT EPR nutation technique. The SCRP signals were partially separated from free-radical signals in the 2D EPR spectrum; SCRP showed additional higher and lower nutation frequencies compared with those of the free radical. Theoretical analyses, including off-resonance effects, are made to explain the experimental results.

INTRODUCTION

During the past decade, many attempts to study spin-correlated radical pairs (SCRP) (*1–4*), generated by flash photolysis of an appropriate precursor, have been made. Recently developed Fourier-transform EPR spectroscopy (*5*) has begun to yield detailed information about kinetics and structures of SCRP as well as other transient species with the aid of its excellent time and frequency resolution and sensitivity, although these species have been conventionally studied by means of the continuous wave time-resolved (CW TR) EPR technique. However, the most remarkable feature of Fourier spectroscopy is the possibility to extend it to multiple dimensions and manipulate pulse sequences to give more detailed information about a spin system. In NMR, many kinds of multidimensional spectroscopies have been successfully developed (*6*). On the contrary, in EPR, only a few two-dimensional EPR experiments, for instance, 2D exchange spectroscopy, are reported (*7, 8*).

When one designs a new experiment of pulsed magnetic resonance, one should focus attention on the spin Hamiltonian as well as on the initial population of a spin system. From this point of view, the SCRP is an interesting topic for 2D EPR spectroscopy. First, an exchange interaction between two radicals exists within the lifetime of the pair. This interaction can be analogous to a scalar spin–spin coupling between nuclear spins in high-resolution NMR in liquid. Second, since the SCRP is created from a singlet or a triplet precursor, it is in a nonequilibrium spin state (*spin correlation*).

It has been shown by Moore *et al.* (*9*) and Dinse *et al.* (*10*) that these peculiarities of SCRPs lead to an anomalous flip-angle dependence of the FT EPR spectrum. Similar situations frequently occur in the study of chemically induced dynamic nuclear polarization (CIDNP) by FT NMR, and the general theory has been given by Ernst and his associates (*11*). According to Dinse's theory, signal intensities of free radicals are proportional to $\sin\beta$, whereas those of the SCRP are proportional to $\sin(2\beta)$, where β is the flip angle of the microwave (MW) pulse. Nutation frequencies of the SCRP are therefore expected to be twice those of free radicals.

Moore *et al.* have reported experimental demonstration of this phenomenon in the study of a photo-induced electron transfer reaction for the carotenoid-porphyrin-quinone linked system (*9*). They compared the intensity of the FT EPR signal at on-resonance position for a set of various microwave field strengths.

In this contribution, we report experimental confirmation of the flip-angle dependence of the SCRP signal in the photo-induced hydrogen-abstraction reaction of acetone with 2-propanol, by means of 2D FT EPR nutation spectroscopy. Many studies have been reported for this system (*4, 16, 17*), and it has been demonstrated that various kinds of chemically induced dynamic electron polarization (CIDEP) mechanisms contribute to the temperature dependence of the EPR spectra. Especially at lower temperatures, SCRP CIDEP is detected at an early time after the laser excitation, accompanied by free radical CIDEP due to the $S - T_0$ and $S - T_-$ mixings by the radical pair mechanism (RPM). We were able to examine the flip-angle dependence of SCRP signals and free-radical signals in the FT EPR spectra by varying the delay time from the laser pulse.

EXPERIMENTS AND DATA PROCESSING

X-band FT EPR measurements were performed with a Bruker ESP-380E spectrometer. Homogeneous and strong MW fields were obtained with a dielectric resonator of sapphire. The sample, 1 mol dm^{-3} solution of acetone-d_6 in 2-

* To whom correspondence should be addressed.

1064-1858/95 $12.00

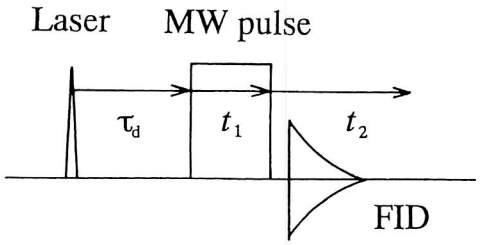

FIG. 1. Pulse sequence for the 2D FT EPR nutation experiment: a MW pulse is synchronized to the laser pulse. When t_1 is changed in a stepwise manner, the FID signal is acquired along t_2.

propanol-d_8, was irradiated by the fourth harmonic (266 nm) of a Spectra-Physics Quanta-Ray GCR-14S Nd:YAG laser with a repetition rate of 10 Hz. In order to introduce the excitation laser pulses, the variable temperature apparatus was modified for pulsed EPR measurements. The temperature was controlled by a Bruker B-VT2000. The sample temperature was measured by a thermocouple and maintained at 185 K by flowing cold N_2 gas. The pulsed EPR experiment was made by utilizing one MW pulse synchronized to the laser pulse. Noticeble depletion of the sample was not observed throughout the experiment.

In the one-dimensional experiment, the duration and the field strength of the MW pulse were about 10 ns and 0.6 mT, respectively. The quadrature free induction decay was recorded in steps of 10 ns by 512 steps with CYCLOPS phase cycling. In order to obtain information about the phase and to avoid distortion of spectra, a missing part of the FID during the instrumental dead time, about 88 ns, was extrapolated with the LPQRD method (*15*). The phase of FT EPR spectra showing CIDEP effects was corrected according to the phase of the spectra at thermal spin equilibrium.

A two-dimensional nutation experiment was designed as shown in Fig. 1 (*12–14*). After the laser pulse, a MW pulse was applied during t_1 and the subsequent quadrature FID was sampled along t_2. This experiment was repeated for a series of various t_1 values, giving a 2D complex FID $S(t_1, t_2)$, which was Fourier-transformed in both dimensions to yield the 2D nutation spectrum $S(\omega_1, \omega_2)$. Here, ω_1 and ω_2 are a nutation frequency and an ordinary EPR frequency, respectively. The duration of the MW pulse, t_1, is incremented in 64 steps of 8 ns and the FID was sampled in 128 steps of 10 ns with an acquisition time of about an hour. The spectra were obtained at two different time delays, 500 ns and 8 μs after the laser excitation. Other settings, except for the MW field strength, were the same as those in the 1D experiment. The complex 2D FIDs were apodized with a Hanning window in each dimension and zero-filled to 256 $\times$ 512 matrices prior to the Fourier transformation.

RESULTS

1D Experiments

One-dimensional FT EPR spectra with various delay times τ_d are shown in Fig. 2. The central hyperfine line of the

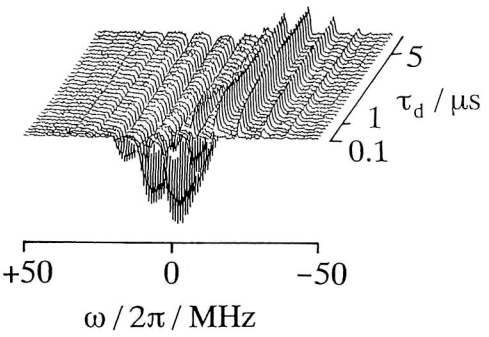

FIG. 2. One-dimensional FT EPR spectra of the acetone-d_6/2-propanol-d_8 system taken at −88°C with various delay times τ_d. The spectra are obtained after reconstruction of the missing part of the FID and subsequent Fourier transformation. The signals of the SCRP are seen with a range of τ_d from 100 ns to 3 μs as the remarkable patterns of antiphased doublet feature.

spectra at early times (from 100 ns to 3 μs) shows the pattern of an emission/absorption (E/A) antiphase doublet. These signals are attributed to SCRP CIDEP signals as already reported by CW TR EPR studies in this system (*16, 17*). These signals increased up to 1 μs and decayed within 3 μs after the laser excitation. The rise and decay of the free-radical component were slower than those of SCRP. Partial expansions of the spectra with the delay times of 500 ns and 8 μs are also presented in Fig. 3.

2D Nutation Experiments

Two-dimensional nutation spectra observed at different delay times of 500 ns and 8 μs are shown in Fig. 4 in absolute-value representation. The contour plots of these spectra are given in Fig. 5. Two important features of these 2D nutation spectra should be noted. First, the peaks (Group A) having the same EPR frequencies and nutation frequencies were observed in the spectra with the delay times of both 500 ns and 8 μs. Second, there were relatively broad

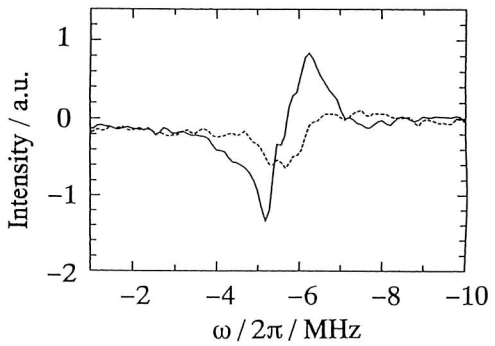

FIG. 3. Partial expansion of the 1D FT EPR spectra, displayed in Fig. 2, with delay times of 500 ns (solid line) and 8 μs (broken line). An antiphase doublet signal, attributed to SCRP CIDEP, appears in the spectrum for 500 ns.

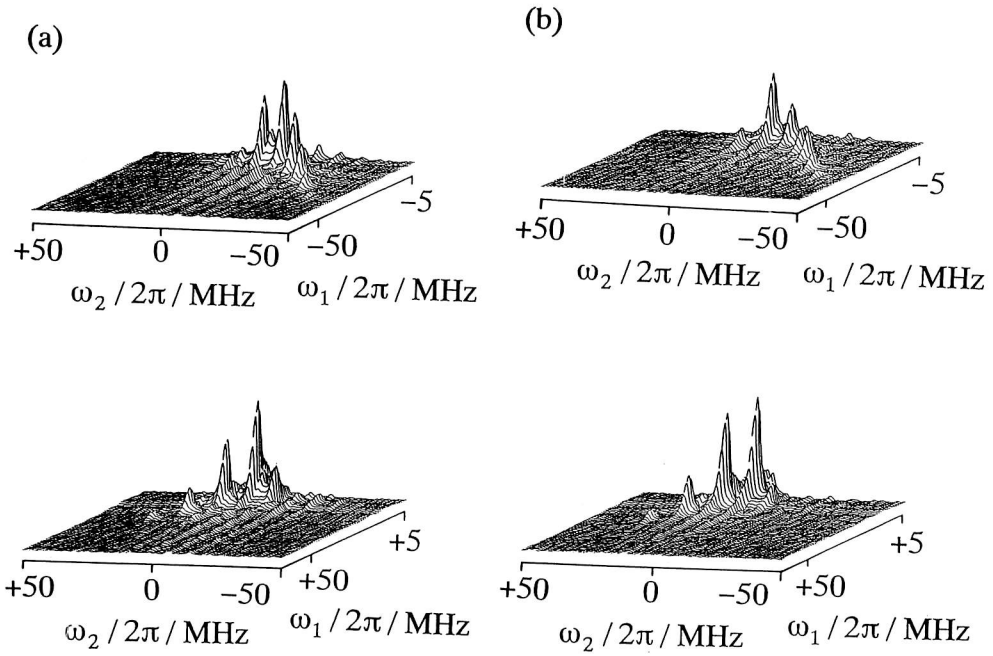

FIG. 4. Absolute value 2D FT EPR nutation spectra of the acetone-d_6/2-propanol-d_8 system at −88°C. Time delays from the laser excitation are 500 ns (a) and 8 μs (b). Here, ω_1 and ω_2 are the nutation frequency and EPR frequency, respectively.

and weak peaks that appeared in a higher-nutation-frequency region (Group B) and also in a lower-nutation-frequency region (Group C) in the spectrum at 500 ns. In Fig. 6, these three groups are clearly labeled.

THEORY AND DISCUSSION

According to the theory proposed by Dinse and co-workers, higher nutation frequencies are expected to be observed for SCRP than for free radicals. However, the existence of peaks with lower nutation frequencies (Group C) could not be explained by their theory. On the other hand, as shown by Ernst *et al.*, the anomalous flip-angle dependence of the FT spectrum is observed only when a spin system is homogeneously excited by an excitation pulse. For high-resolution NMR in liquid, this situation holds good because of the relatively narrow spectral bandwidth. In EPR, however, it is difficult to excite the whole spectrum homogeneously by the MW pulse. Thus, in the 2D nutation experiments in EPR, we must consider off-resonance effects.

Off-Resonance Effects for Nutation Frequencies of the Isolated Radical

If we neglect spin relaxation and development of spin polarization, the spin dynamics is governed by nutation and precession during the MW pulse. In the case of an isolated radical, the density-matrix theory is completely reduced to the treatment of the Bloch equations (*18*). In a reference frame rotating with the frequency of the MW source, the magnetization rotates about an effective field, which depends on the resonance offset Ω. The effective field B_{eff} is determined by the hypothetical offset field

$$\Delta B = \frac{\Omega}{\gamma} \qquad [1]$$

along the longitudinal axis and by the MW field B_1 in the transverse plane (Fig. 7) as expressed by

$$B_{\text{eff}} = \sqrt{B_1^2 + \Delta B^2} \qquad [2]$$

and its tilt angle θ is given by

$$\tan \theta = \frac{B_1}{\Delta B}. \qquad [3]$$

The nutation frequency ω under the MW pulse is given by

$$\omega = \gamma B_{\text{eff}}. \qquad [4]$$

It should be noted that the nutation frequency increases with increasing resonance offset Ω. When the MW field lies along the $-y$ axis, transverse magnetization immediately after the MW pulse with duration of t_1 is proportional to

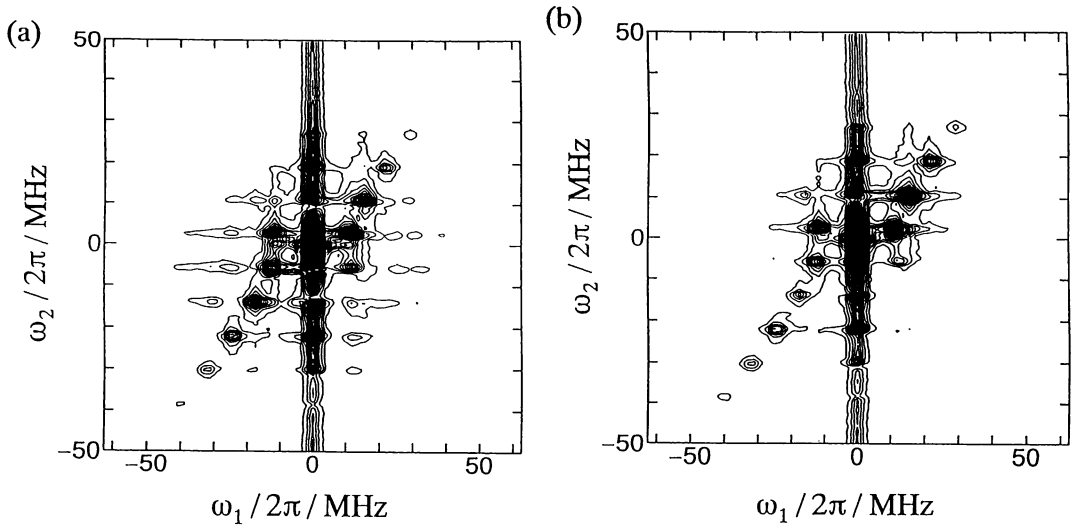

FIG. 5. Contour plots of Fig. 4. Delay times are 500 ns (a) and 8 μs (b), respectively. The peaks with the higher and lower nutation frequencies appear in the spectrum for 500 ns, compared with the nutation frequencies of peaks in that for 8 μs. Strong components of $\omega_1 = 0$ were caused by an experimental artifact.

$$\sin\theta\{\sin\omega t_1 + i\cos\theta(1 - \cos\omega t_1)\}. \quad [5]$$

The factor of $\cos\theta$ leads to an asymmetry in the nutation spectrum with respect to $\omega = 0$ and the intensity ratio of the $+\omega$ to $-\omega$ peaks is determined by this factor. The nutation spectrum obtained at the delay of 8 μs, when no SCRP was detected in the 1D spectrum, can be interpreted by the above theory. We therefore conclude that there exists only the z magnetization of the free radical at 8 μs from both the 1D and the 2D experiments.

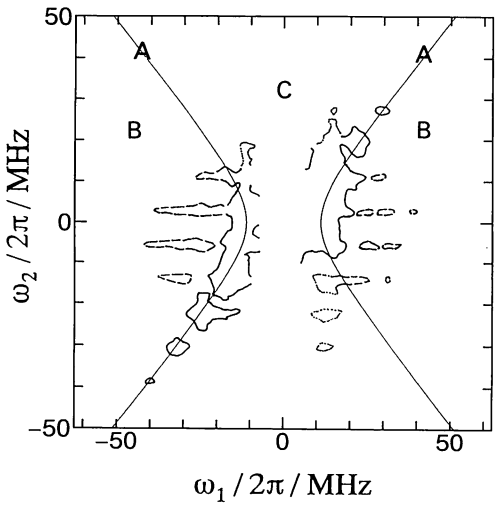

FIG. 6. Labeling of the groups of peaks A, B, and C in Fig. 5a. The Group A peaks are surrounded by solid lines, the Group B broken lines, and the Group C dotted lines. Correlation between EPR frequency and nutation frequency in the Group A peaks is also depicted.

Nutation Behavior of the SCRP Signal

When we take into account only nutation and precession under a constant exchange interaction, the time evolution of a spin-density operator σ in the rotating frame is expressed from the well-known Liouville–von Neumann equation (*19*) as

$$\sigma(t_1, t_2) = \exp(-i\mathcal{H}_0 t_2)\exp[-i(\mathcal{H}_0 + \mathcal{H}_p)t_1] \times \sigma(0)\exp[i(\mathcal{H}_0 + \mathcal{H}_p)t_1]\exp(i\mathcal{H}_0 t_2). \quad [6]$$

Here $\mathcal{H}_0$ is the unperturbed Hamiltonian of the SCRP, $\mathcal{H}_p$ is the perturbed Hamiltonian that expresses an interaction with the MW pulse in the rotating frame, and t_1 and t_2 are evolution times with and without the MW pulse, respectively.

When the high-field approximation is valid, the isotropic spin Hamiltonian of the SCRP in the laboratory frame (*4*) is expressed by

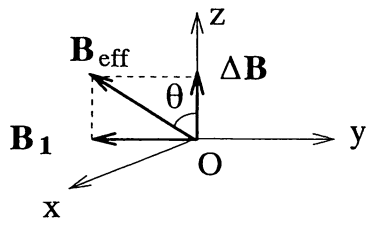

FIG. 7. Effective magnetic field in the rotating frame. The effective field $\mathbf{B}_{eff}$, a composite vector of $\mathbf{B}_1$ and $\Delta\mathbf{B}$, is displayed for a case where an applied MW field $\mathbf{B}_1$ lies along the negative y axis.

$$\mathcal{H}_0 = \gamma_a B_0 S_{az} + \gamma_b B_0 S_{bz} + \sum_m A_{am} S_{az} I_{amz} + \sum_n A_{bn} S_{bz} I_{bnz} - J\left(2\mathbf{S}_a \cdot \mathbf{S}_b + \frac{1}{2}\right), \quad [7]$$

where J is an isotropic exchange interaction between two radicals a and b, and other symbols have their usual meanings. The spin Hamiltonian in the rotating frame is rewritten as

$$\mathcal{H}_0 = \Omega_a S_{az} + \Omega_b S_{bz} - J(2\mathbf{S}_a \cdot \mathbf{S}_b + \tfrac{1}{2}), \quad [8]$$

which is spanned by the electron-spin basis. Here Ω_a and Ω_b represent the offset frequencies of electron spins a and b in the reference frame, respectively. On the other hand, when the MW field is along the negative y axis in this frame, $\mathcal{H}_p$ is written as

$$\mathcal{H}_p = -\gamma_a B_1 S_{ay} - \gamma_b B_1 S_{by}. \quad [9]$$

The two-dimensional FID is calculated as functions of t_1 and t_2:

$$S(t_1, t_2) = \mathrm{tr}\{\sigma(t_1, t_2)(S_x + iS_y)\}. \quad [10]$$

Incidentally, the calculation of the exponential operator $\exp[i(\mathcal{H}_0 + \mathcal{H}_p)t_1]$ requires diagonalization of a 4×4 Hermitian matrix and must be performed numerically. In this paper, we obtain a series of analytical expressions for the nutation frequencies of the SCRP by utilizing the two assumptions that the exchange interaction is much smaller than both the interaction of the spin system with the MW field and the difference in the offset frequencies of two electron spins. Under the first approximation, the spin Hamiltonian during the MW pulse is almost equal to a sum of the Hamiltonians of two electron spins, namely,

$$\mathcal{H}_p + \mathcal{H}_0 \approx \mathcal{H}_a + \mathcal{H}_b, \quad [11]$$

where

$$\mathcal{H}_a = -\gamma_a B_1 S_{ay} + \Omega_a S_{az}, \quad [12]$$

$$\mathcal{H}_b = -\gamma_b B_1 S_{by} + \Omega_b S_{bz}. \quad [13]$$

Because $[\mathcal{H}_a, \mathcal{H}_b] = 0$,

$$\exp[i(\mathcal{H}_p + \mathcal{H}_0)t_1] = \exp[i(\mathcal{H}_a + \mathcal{H}_b)t_1] = \exp(i\mathcal{H}_a t_1)\exp(i\mathcal{H}_b t_1), \quad [14]$$

where $\exp(i\mathcal{H}_a t_1)$ and $\exp(i\mathcal{H}_b t_1)$ can be derived analytically. If we let T_a be the unitary transformation which diagonalizes $\mathcal{H}_a$, and E_a be the diagonalized operator, i.e.,

$$E_a = T_a^{-1}\mathcal{H}_a T_a, \quad [15]$$

we obtain

$$\exp(i\mathcal{H}_a t_1) = T_a^{-1}\exp(iE_a t_1)T_a = \begin{bmatrix} \left(\cos^2\frac{\theta_a}{2}\right)\exp\left(\frac{i}{2}\omega_a t_1\right) + \left(\sin^2\frac{\theta_a}{2}\right)\exp\left(-\frac{i}{2}\omega_a t_1\right) & -\sin\theta_a \sin\left(\frac{1}{2}\omega_a t_1\right) \\ \sin\theta_a \sin\left(\frac{1}{2}\omega_a t_1\right) & \left(\sin^2\frac{\theta_a}{2}\right)\exp\left(\frac{i}{2}\omega_a t_1\right) + \left(\cos^2\frac{\theta_a}{2}\right)\exp\left(-\frac{i}{2}\omega_a t_1\right) \end{bmatrix} \quad [16]$$

with the tilt angle θ_a for the effective field of spin a in the rotating frame as

$$\tan\theta_a = \frac{\gamma_a B_1}{\Omega_a} = \frac{B_1}{\Delta B_a} \quad [17]$$

and with the nutation frequency

$$\omega_a = \sqrt{\Omega_a^2 + (\gamma_a B_1)^2}. \quad [18]$$

In the same way, we derive the matrix for $\exp(i\mathcal{H}_b t_1)$, and the tensor product $\exp(i\mathcal{H}_a t_1) \otimes \exp(i\mathcal{H}_b t_1)$ is calculated. Under the second assumption we obtain

$$|\Omega_a - \Omega_b| \gg |J|. \quad [19]$$

In this limit, as four eigenstates of the unperturbed Hamiltonian $\mathcal{H}_0$ are not so far from the product bases, $\alpha\alpha$, $\alpha\beta$, $\beta\alpha$, $\beta\beta$, the initial density matrix is regarded to be

$$\sigma(0) = \begin{array}{c} \begin{matrix} \alpha\alpha & \alpha\beta & \beta\alpha & \beta\beta \end{matrix} \\ \begin{bmatrix} A & & & \\ & B & & \\ & & C & \\ & & & D \end{bmatrix} \end{array}. \quad [20]$$

If the density matrix just after the MW pulse is expressed as

$$\sigma(t_1, 0) = [\exp(i\mathcal{H}_a t_1) \otimes \exp(i\mathcal{H}_b t_1)]^{-1} \times \sigma_0[\exp(i\mathcal{H}_a t_1) \otimes \exp(i\mathcal{H}_b t_1)] = \begin{array}{c} \begin{matrix} \alpha\alpha & \alpha\beta & \beta\alpha & \beta\beta \end{matrix} \\ \begin{bmatrix} E & F & G & H \\ I & J & K & L \\ M & N & O & P \\ Q & R & S & T \end{bmatrix} \end{array}, \quad [21]$$

with the assumption of the small exchange integral, time evolution during t_2 yields the density matrix (*10*)

$$\sigma(t_1, t_2) = \begin{array}{c} \begin{matrix} \alpha\alpha & \alpha\beta & \beta\alpha & \beta\beta \end{matrix} \\ \begin{bmatrix} E & F\exp[-i(\Omega_b - J)t_2] & G\exp[-i(\Omega_a - J)t_2] & H\exp[-i(\Omega_a + \Omega_b)t_2] \\ I\exp[i(\Omega_b - J)t_2] & J & K\exp[-i(\Omega_a - \Omega_b)t_2] & L\exp[-i(\Omega_a + J)t_2] \\ M\exp[i(\Omega_a - J)t_2] & N\exp[i(\Omega_a - \Omega_b)t_2] & O & P\exp[-i(\Omega_b + J)t_2] \\ Q\exp[i(\Omega_a + \Omega_b)t_2] & R\exp[i(\Omega_a + J)t_2] & S\exp[i(\Omega_b + J)t_2] & T \end{bmatrix} \end{array}. \quad [22]$$

Since the 2D FID obtained by Eq. [10] is expressed as

$$s(t_1, t_2) = I\exp[i(\Omega_b - J)t_2] + M\exp[i(\Omega_a - J)t_2] + R\exp[i(\Omega_a + J)t_2] + S\exp[i(\Omega_b + J)t_2], \quad [23]$$

R, M, S, and I determine the nutation frequencies associated with four EPR frequencies of $\Omega_a + J$, $\Omega_a - J$, $\Omega_b + J$, and $\Omega_b - J$, respectively. The calculation of single-quantum coherences gives formulas for the nutation frequencies. The expressions obtained are summarized in Table 1.

It should be noted from these formulas that, in general, four nutation frequencies (except for DC and negative frequencies) are detected in the spin system composed of two spins of $S = \frac{1}{2}$, when the spin–spin coupling is weak. These four frequencies are ω_a, ω_b, $\omega_a + \omega_b$, and $\omega_a - \omega_b$. Among these, ω_a and ω_b are the same nutation frequencies as observed originally when electron spins a and b exist as isolated free radicals, respectively.

As shown in Table 2, in the case of a SCRP coming from the triplet precursor, one can put $A = D = \frac{1}{3}$ and $B = C = \frac{1}{6}$ into Eq. [20] and obtain a series of expressions for the transverse magnetization after the MW pulse. For the transition with the frequency of $\Omega_a + J$, the relative intensity of the ω_a component to the ω_b, $\omega_a + \omega_b$, and $\omega_a - \omega_b$ components is determined only by the tilt angle θ_b that is related to the resonance offset of spin b. On the other hand, when the radical pair is at thermal spin equilibrium at high temperatures, that is, $A - B = A - C = B - D = C - D = -\delta < 0$, the transverse magnetization concerning the EPR transition of spin a right after the MW pulse is expressed by

$$\tfrac{1}{2}\delta \sin\theta_a\{\sin\omega_a t_1 + i\cos\theta_a(1 - \cos\omega_a t_1)\} \quad [24]$$

and similar expressions hold true for the other transitions. From this formula we expect that the nutation frequencies of the radical pair are the same as those for the free radicals.

Next, we consider the nutation frequencies of a SCRP for various combinations of resonance offsets. In the limit where both electron spins are on-resonance, modulation of FID intensities by the MW duration t_1 is given by

$$\pm\tfrac{1}{24}\sin(2\omega t_1). \quad [25]$$

This expression is identical to the formula proposed by Dinse *et al.* giving a nutation frequency of 2ω, where ω is the nutation frequency of the free radical. That is to say, the nutation frequencies expected from Dinse's theory are reasonable only when two electron spins are under an on-resonance condition. In contrast, if only one of the two electron spins is excited, e.g., spin a, transverse magnetization after the MW pulse is expressed by

$$\pm\tfrac{1}{12}\sin\theta_a\{\sin\omega_a t_1 + i\cos\theta_a(1 - \cos\omega_a t_1)\}. \quad [26]$$

In this case, one may observe the same nutation frequencies as those of the free radical (selective excitation effect). This selective excitation effect is hyperfine selective and differs from the spin-selective excitation effect which is popular in NMR.

When we simulate the 2D nutation spectrum of a SCRP, we should consider all combinations of nuclear spin states. Here, the nuclear spin state contributes to the resonance offset of the electron spin. The dominant nutation frequencies for typical combinations of resonance offsets are summarized in Fig. 8. When both electron spins are at almost on-resonance condition, 2ω is observed as the nutation frequency that contributes to a nutation frequency higher than that of free radicals in the 2D spectrum. On the other hand, when spin a is near the resonance condition and spin b is far from on-resonance, the nutation frequency for the transitions of a is expected to

TABLE 1

Expressions for the Transverse Magnetization Immediately after the MW Pulse for a Spin System Composed of Two Spins of $S = \frac{1}{2}$

EPR frequency	Transverse magnetization just after the MW pulse
$\Omega_a + J$	$\frac{1}{2}\sin\theta_a[\{(1 - \frac{1}{2}\sin^2\theta_b)(D - B) + \frac{1}{2}\sin^2\theta_b(C - A)\}\{\sin\omega_a t_1 + i\cos\theta_a(1 - \cos\omega_a t_1)\}$ $+ \frac{1}{4}\{(D - B) - (C - A)\}\sin^2\theta_b\{\sin(\omega_a - \omega_b)t_1 + i\cos\theta_b\{\cos\omega_b t_1 - \cos(\omega_a - \omega_b)t_1\}$ $+ \sin(\omega_a + \omega_b)t_1 + i\cos\theta_b\{\cos\omega_b t_1 - \cos(\omega_a + \omega_b)t_1\}\}]$
$\Omega_a - J$	$\frac{1}{2}\sin\theta_a[\{(1 - \frac{1}{2}\sin^2\theta_b)(C - A) + \frac{1}{2}\sin^2\theta_b(D - B)\}\{\sin\omega_a t_1 + i\cos\theta_a(1 - \cos\omega_a t_1)\}$ $+ \frac{1}{4}\{(C - A) - (D - B)\}\sin^2\theta_b\{\sin(\omega_a - \omega_b)t_1 + i\cos\theta_b\{\cos\omega_b t_1 - \cos(\omega_a - \omega_b)t_1\}$ $+ \sin(\omega_a + \omega_b)t_1 + i\cos\theta_b\{\cos\omega_b t_1 - \cos(\omega_a + \omega_b)t_1\}\}]$
$\Omega_b + J$	$\frac{1}{2}\sin\theta_b[\{(1 - \frac{1}{2}\sin^2\theta_a)(D - C) + \frac{1}{2}\sin^2\theta_a(B - A)\}\{\sin\omega_b t_1 + i\cos\theta_b(1 - \cos\omega_b t_1)\}$ $+ \frac{1}{4}\{(D - C) - (B - A)\}\sin^2\theta_a\{\sin(\omega_b - \omega_a)t_1 + i\cos\theta_a\{\cos\omega_a t_1 - \cos(\omega_b - \omega_a)t_1\}$ $+ \sin(\omega_b + \omega_a)t_1 + i\cos\theta_a\{\cos\omega_a t_1 - \cos(\omega_b + \omega_a)t_1\}\}]$
$\Omega_b - J$	$\frac{1}{2}\sin\theta_b[\{(1 - \frac{1}{2}\sin^2\theta_a)(B - A) + \frac{1}{2}\sin^2\theta_a(D - C)\}\{\sin\omega_b t_1 + i\cos\theta_b(1 - \cos\omega_b t_1)\}$ $+ \frac{1}{4}\{(B - A) - (D - C)\}\sin^2\theta_a\{\sin(\omega_b - \omega_a)t_1 + i\cos\theta_a\{\cos\omega_a t_1 - \cos(\omega_b - \omega_a)t_1\}$ $+ \sin(\omega_b + \omega_a)t_1 + i\cos\theta_a\{\cos\omega_a t_1 - \cos(\omega_b + \omega_a)t_1\}\}]$

Note. The meanings of the symbols are defined in the text.

be ω_a, and those of electron spin b are ω_a (instead of ω_b), $\omega_b + \omega_a$, $\omega_b - \omega_a$. Since ω_a is the nutation frequency of electron spin a and the resonance offset of a is smaller than that of spin b, this frequency ω_a is lower than the nutation frequency ω_b. Consequently, in this case the ω_a and the $\omega_b - \omega_a$ components contribute to the lower nutation frequencies. Moreover, when both electron spins are far from the on-resonance condition, the nutation frequencies of both electron spins are equal to those of the free radicals.

In the 2D nutation spectrum at 500 ns after the laser excitation, two components having higher (Group B) and lower (Group C) nutation frequencies were newly observed. The Group B

TABLE 2

Transverse Magnetization Immediately after the MW pulse for SCRP Coming from a Triplet Precursor

EPR frequency	Transverse magnetization after the MW pulse
$\Omega_a + J$	$\frac{1}{12}\sin\theta_a[\cos^2\theta_b\{\sin\omega_a t_1 + i\cos\theta_a(1 - \cos\omega_a t_1)\}$ $+ \frac{1}{2}\sin^2\theta_b\{\sin(\omega_a - \omega_b)t_1 + i\cos\theta_b\{\cos\omega_b t_1 - \cos(\omega_a - \omega_b)t_1\}$ $+ \sin(\omega_a + \omega_b)t_1 + i\cos\theta_b\{\cos\omega_b t_1 - \cos(\omega_a + \omega_b)t_1\}\}]$
$\Omega_a - J$	$-\frac{1}{12}\sin\theta_a[\cos^2\theta_b\{\sin\omega_a t_1 + i\cos\theta_a(1 - \cos\omega_a t_1)\}$ $+ \frac{1}{2}\sin^2\theta_b\{\sin(\omega_a - \omega_b)t_1 + i\cos\theta_b\{\cos\omega_b t_1 - \cos(\omega_a - \omega_b)t_1\}$ $+ \sin(\omega_a + \omega_b)t_1 + i\cos\theta_b\{\cos\omega_b t_1 - \cos(\omega_a + \omega_b)t_1\}\}]$
$\Omega_b + J$	$\frac{1}{12}\sin\theta_b[\cos^2\theta_a\{\sin\omega_b t_1 + i\cos\theta_b(1 - \cos\omega_b t_1)\}$ $+ \frac{1}{2}\sin^2\theta_a\{\sin(\omega_b - \omega_a)t_1 + i\cos\theta_a\{\cos\omega_a t_1 - \cos(\omega_b - \omega_a)t_1\}$ $+ \sin(\omega_b + \omega_a)t_1 + i\cos\theta_a\{\cos\omega_a t_1 - \cos(\omega_b + \omega_a)t_1\}\}]$
$\Omega_b - J$	$-\frac{1}{12}\sin\theta_b[\cos^2\theta_a\{\sin\omega_b t_1 + i\cos\theta_b(1 - \cos\omega_b t_1)\}$ $+ \frac{1}{2}\sin^2\theta_a\{\sin(\omega_b - \omega_a)t_1 + i\cos\theta_a\{\cos\omega_a t_1 - \cos(\omega_b - \omega_a)t_1\}$ $+ \sin(\omega_b + \omega_a)t_1 + i\cos\theta_a\{\cos\omega_a t_1 - \cos(\omega_b + \omega_a)t_1\}\}]$

Note. These expressions are obtained by substituting $A = D = \frac{1}{3}$ and $B = C = \frac{1}{6}$ into the formulas in Table 1.

Combination of Resonance Offsets	Transition of Spin *a*	Transition of Spin *b*
a *b*	$\omega_a + \omega_b$ ($\approx 2\omega$)	$\omega_a + \omega_b$ ($\approx 2\omega$)
a *b*	ω_a	ω_a $\omega_a + \omega_b$ $\omega_a - \omega_b$
a *b*	ω_a	ω_b
a *b*	ω_a	ω_b

FIG. 8. Typical nutation frequencies for a SCRP in some combination of resonance offsets, obtained by the formulas shown in Table 2. Broken lines indicate on-resonance positions. The presence of DC components is not shown.

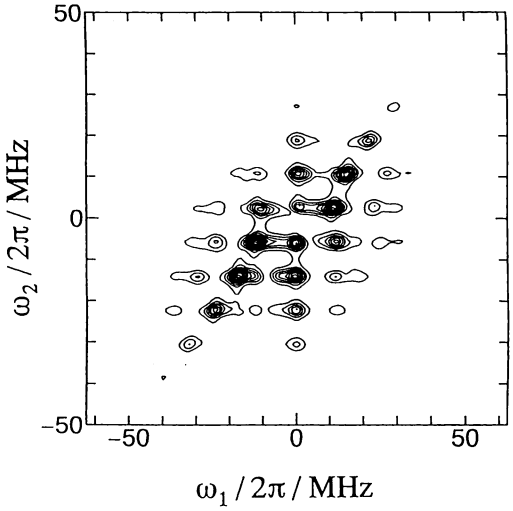

FIG. 9. Calculated 2D FT EPR nutation spectrum of the acetone ketyl radical pair created from the triplet precursor. No contribution from the free radical CIDEP was taken into consideration. Parameters used here are tabulated in Table 3.

peaks appeared close to the on-resonance condition and have nutation frequencies twice those of the free radicals. These peaks are assigned to arise from the combinations of hyperfine lines with small resonance offsets, and, therefore, these peaks have higher nutation frequencies. On the contrary, the Group C peaks are positioned far from the on-resonance condition, having nutation frequencies lower than those expected for the isolated electron spins of hyperfine lines with large resonance offsets. These peaks are thought to come from the combinations between the hyperfine lines with small resonance offset and that with large resonance offset. In this case, as discussed above, one of the nutation frequencies of the spin, being far from the resonance condition, is expected to be the same as that originally observed for the isolated partner spin. Hence, the lower nutation frequencies of Group C peaks are attributed to the partner hyperfine lines positioned close to on-resonance. When we sum up all the nuclear configurations, the statistical weighting factors of hyperfine lines centered in the spectrum are much larger than those of the others. Therefore, contributions from combinations involving the hyperfine lines centered in the spectrum seem to be dominant. Relative intensities of peaks with the sum and the difference nutation frequencies of two spins must be too weak to be detected. Consequently, the Group B and the Group C peaks give direct evidence that the spin system is composed of two electron spins and lies in a nonequilibrium state. On the other hand, the Group A peaks in the spectrum at 500 ns may contain considerable contributions from SCRP signals, although the nutation frequencies of the Group A peaks equal those of free radicals.

TABLE 3
Parameters Used in the Calculation of 2D FT EPR Nutation Spectrum of Fig. 8

Parameter	Value
$\Omega/2\pi$*	−5.70 MHz
$A(CD_3)/2\pi$	8.205 MHz
$A(OD)/2\pi$	0.327 MHz
$J/2\pi$	−0.560 MHz
B_1	0.390 mT
$g_a = g_b$	2.0037

* Offset frequency of the center of the spectrum.

Finally, we try to simulate the observed 2D nutation spectrum of a SCRP. According to the aforementioned theory, we can numerically solve the time evolution of the spin density matrix without neglecting the exchange interaction J. In the case of a triplet precursor, an initial density matrix has off-diagonal elements in the eigenbasis, ψ_1, ψ_2, ψ_3, and ψ_4, of the unperturbed Hamiltonian $\mathcal{H}_0$ (zero-quantum coherences, ZQC). For the case of the SCRP in liquid, ZQC will rapidly disappear during the early time of photochemical reactions to give an incoherent state, due to effective fluctuations of J. Hence, we adopted the density matrix before the MW pulse as

$$\sigma(0) = \begin{array}{c} \begin{matrix} \psi_1 & \psi_2 & \psi_3 & \psi_4 \end{matrix} \\ \begin{bmatrix} \frac{1}{3} & & & \\ & \frac{1}{3}\sin^2\Theta & & \\ & & \frac{1}{3}\cos^2\Theta & \\ & & & \frac{1}{3} \end{bmatrix} \end{array}, \qquad [27]$$

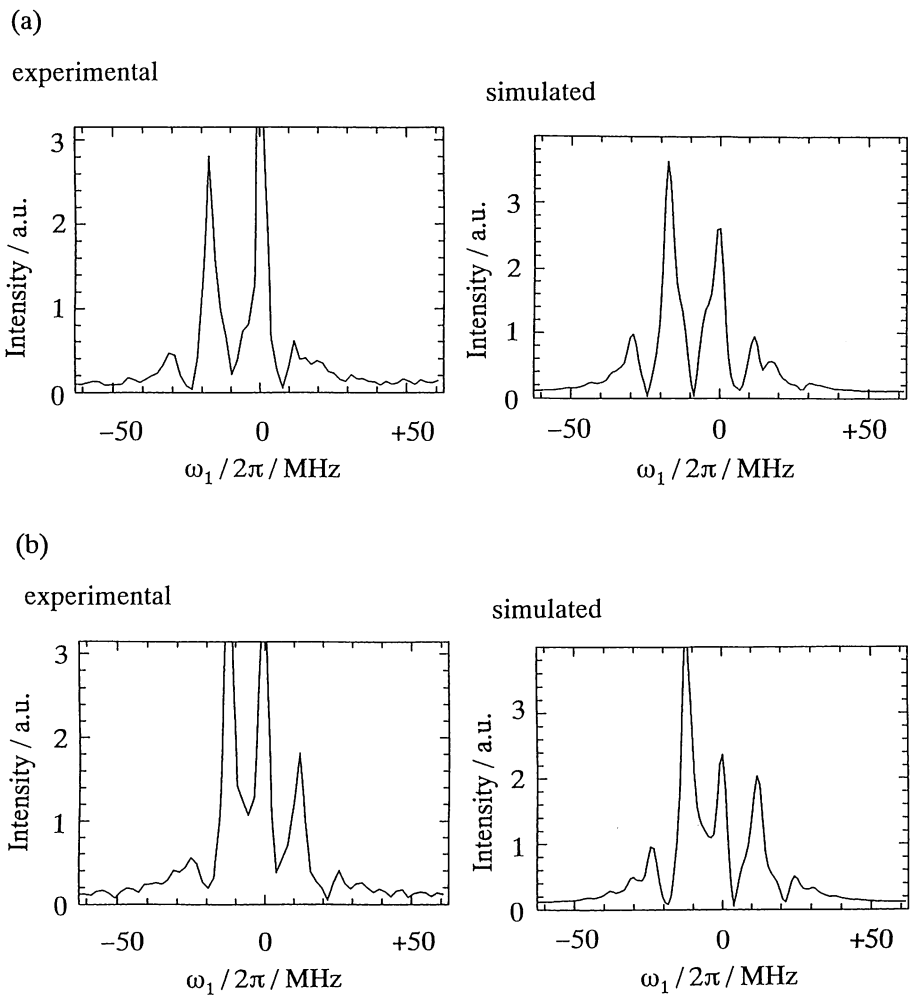

FIG. 10. Slices of the observed 2D spectrum along two EPR frequencies ω_2 at the delay time of 500 ns and the calculated spectrum displayed in Fig. 8: (a) $\omega_2/2\pi = -14.1$ MHz and (b) $\omega_2/2\pi = -5.5$ MHz.

where

$$\psi_1 = |T_+\rangle, \quad [28]$$

$$\psi_2 = \cos\Theta|S\rangle + \sin\Theta|T_0\rangle, \quad [29]$$

$$\psi_3 = -\sin\Theta|S\rangle + \cos\Theta|T_0\rangle, \quad [30]$$

$$\psi_4 = |T_-\rangle, \quad [31]$$

$$Q = \langle S|\mathcal{H}_0|T_0\rangle, \quad [32]$$

$$\tan(2\Theta) = Q/J. \quad [33]$$

The calculated 2D nutation spectrum of the acetone ketyl radical pair is shown in Fig. 9. Parameters used in the calculation of the 2D FT EPR nutation spectrum are listed in Table 3. This spectrum does not contain any contribution from the free radical. Correlation of the observed nutation and EPR frequencies of the Group B and Group C peaks are fairly well reproduced. In addition, the nutation spectra sliced along two EPR frequencies, $\omega_2 = -14.1$ and -5.5 MHz (Fig. 10), give rise to similar intensity ratio at each peak to that of the experimentally obtained spectrum.

CONCLUDING REMARKS

Two-dimensional EPR nutation experiments were performed in order to verify the anomalous flip-angle dependence of the FT EPR spectra of photochemically generated SCRP. In comparison with the later spectrum where no SCRP was detected, new peaks were observed in an earlier 2D nutation spectrum which were assigned as those of SCRP. The frequencies of these peaks are higher and lower than those of the free radicals. The peaks of the higher nutation frequencies are simply explained by Dinse's treatment. On the other hand, the peaks of the

lower nutation frequencies were not explained without consideration of the off-resonance effect.

In this 2D spectroscopy, the SCRP signal was partially separated from the free-radical signal for the first time and gave direct spectroscopic evidence of spin correlation in the transient radical pair.

ACKNOWLEDGMENTS

This work was supported by Grants-in-Aid for Scientific Research 06640711 (M.I.), 04242102 (S.Y.), and 06239208 (S.Y.) from the Ministry of Education, Science, and Culture of Japan. The authors are grateful to Professor Dr. Shozo Tero-Kubota for his help in the FT-EPR measurements and also to Mr. Hiroshi Yamada for the construction of the variable temperature apparatus.

REFERENCES

1. M. C. Thurnauer, M. K. Bowman, and J. R. Norris, *FEBS Lett.* **100,** 309 (1979).
2. M. C. Thurnauer and J. R. Norris, *Chem. Phys. Lett.* **76,** 557 (1980).
3. M. C. Thurnauer, A. W. Rutherford, and J. R. Norris, *Biochem. Biophys. Acta* **682,** 332 (1982).
4. C. D. Buckley, D. A. Hunter, P. J. Hore, and K. A. McLauchlan, *Chem. Phys. Lett.* **135,** 307 (1987).
5. L. Kevan and M. K. Bowman (Eds.), "Modern Pulsed and Continuous Wave Electron Spin Resonance," Wiley, New York, 1990.
6. R. R. Ernst, G. Bodenhausen, and A. Wokaun (Eds.), "Principles of Nuclear Magnetic Resonance in One and Two Dimensions," Oxford, New York, 1987.
7. J. Gorcester and J. H. Freed, *J. Chem. Phys.* **85,** 5375 (1986).
8. A. Angerhofer, R. J. Massoth, and M. K. Bowman, *Isr. J. Chem.* **28,** 227 (1988).
9. K. Harashanori, H. Levanon, J. Tang, M. K. Bowman, J. R. Norris, D. Gust, T. A. Moore, and A. L. Moore, *J. Am. Chem. Soc.* **112,** 6477 (1990).
10. G. Kroll, M. Plüschau, K.-P. Dinse, and H. van Willigen, *J. Chem. Phys.* **93,** 8709 (1990).
11. S. Schäublin, A. Höhner, and R. R. Ernst, *J. Magn. Reson.* **13,** 196 (1974).
12. A. Samoson and E. Lippmaa, *Chem. Phys. Lett.* **100,** 205 (1983).
13. F. M. M. Geurts, A. P. K. Kentgens, and W. S. Veeman, *Chem. Phys. Lett.* **120,** 206 (1985).
14. A. P. M. Kentgens, J. J. Lemmens, F. M. M. Geurts, and W. S. Veeman, *J. Magn. Reson.* **71,** 62 (1987).
15. J. Tang, C. P. Lin, and J. R. Norris, *J. Magn. Reson.* **62,** 167 (1985).
16. K. Tominaga, S. Yamauchi, and N. Hirota, *J. Chem. Phys.* **88,** 553 (1988).
17. K. Tominaga, S. Yamauchi, and N. Hirota, *J. Chem. Phys.* **92,** 5157 (1990).
18. H. C. Torrey, *Phys. Rev.* **76,** 1059 (1949).
19. U. Fano, *Rev. Mod. Phys.* **29,** 74 (1957).